
GAITMAST: MOTION-AWARE SPATIO-TEMPORAL FEATURE LEARNING NETWORK FOR CROSS-VIEW GAIT RECOGNITION

Jingqi Li¹, Jiaqi Gao¹, Yuzhen Zhang¹, Hongming Shan¹, Junping Zhang¹

¹Fudan University, Shanghai, China
{lijq20, jqgao20, hmshan, jpzhang}@fudan.edu.cn
yuzhenzhang21@m.fudan.edu.cn

ABSTRACT

As a unique biometric that can be perceived at a distance, gait has broad applications in person authentication, social security and so on. Existing gait recognition methods pay attention to extracting either spatial or spatiotemporal representations. However, they barely consider extracting diverse motion features, a fundamental characteristic in gaits, from gait sequences. In this paper, we propose a novel motion-aware spatiotemporal feature learning network for gait recognition, termed GaitMAST, which can unleash the potential of motion-aware features. In the shallow layer, specifically, we propose a dual-path frame-level feature extractor, in which one path extracts overall spatiotemporal features and the other extracts motion salient features by focusing on dynamic regions. In the deeper layers, we design a two-branch clip-level feature extractor, in which one focuses on fine-grained spatial information and the other on motion detail preservation. Consequently, our GaitMAST preserves the individual's unique walking patterns well, further enhancing the robustness of spatiotemporal features. Extensive experimental results on two commonly-used cross-view gait datasets demonstrate the superior performance of GaitMAST over existing state-of-the-art methods. On CASIA-B, our model achieves an average rank-1 accuracy of 94.1%. In particular, GaitMAST achieves rank-1 accuracies of 96.1% and 88.1% under the bag-carrying and coat-wearing conditions, respectively, outperforming the second best by a large margin and demonstrating its robustness against spatial variations.

1 Related work

Gait recognition: Gait recognition methods can be roughly categorized into the model-based and appearance-based. The model-based methods [1, 2, 3] employ body structures, consisting of individuals' underlying physical characteristics, for feature extraction. One advantage for this category is that it is robust to spatial variations such as camera perspective and personal appearance. Since the skeleton is estimated by the pose estimation methods, however, it is computationally expensive and less precise. Alternatively, appearance-based methods employ binary silhouette maps for better concise silhouette. Early works [4, 5, 6] synthesize a gait template through averaging a set of gait sequences to reduce the input data dimensions. Recent works use silhouette sequences as input [7, 8, 9]. Although the dimension of input sequences is not as low as the gait template, it preserves more kinetic details, thus improving the feature representation richness. A significant difference from existing works is that our appearance-based method takes gait motion into account, which brings considerable performance improvement for gait recognition.

Spatiotemporal modeling: Recent works of literature employ the sequence-level feature as the final gait representation. On one hand, some extract the frame-level feature without considering the temporal relationships, then aggregate the frame-level feature into the sequence-level feature. GaitSet [7] aggregates the frame-level feature by a concise max pool on the temporal dimension, while GaitNet [10] and another work [11] use the LSTM-based integration over time. On the other hand, some consider the temporal relationship in the feature extraction stage. CSTL [12] models the temporal relations after extracting the frame-level feature. Meanwhile, MT3D [13], 3DLocal [14] and GaitGL [9] directly extract the spatiotemporal feature based on 3D convolution, proving that temporal relationships in the sequence are beneficial for gait recognition. A shared insight of this kind of spatiotemporal modeling methods is that they do

not explicitly model the temporal motion, losing the rich walking information. To overcome this issue, we design two modules, one for extracting the motion feature from silhouette sequences with sufficient motion information and the other to preserve the feature’s motion details. Note that MotionGait [15] is a little related to our second module since they also use the temporal difference to obtain the motion-related information. However, the access and utilization of temporal differences are entirely different. First, the difference objection differs since we enlarge the motion search space between adjacent frames. Second, we conduct the bi-directional and multi-granularity temporal differences while they do not. Further, they multiply the original feature with temporal difference directly. Unlike it, we use the temporal difference to compute the motion intensity for recalibrating the motion-related feature.

2 Methodology

This section overviews the proposed GaitMAST and introduces two novel motion-aware modules: frame-level spatiotemporal feature extractor (FLST) and clip-level spatiotemporal feature extractor (CLST). Then, we detail the feature mapping and loss function, followed by the training and testing strategy for GaitMAST.

2.1 Overview of GaitMAST

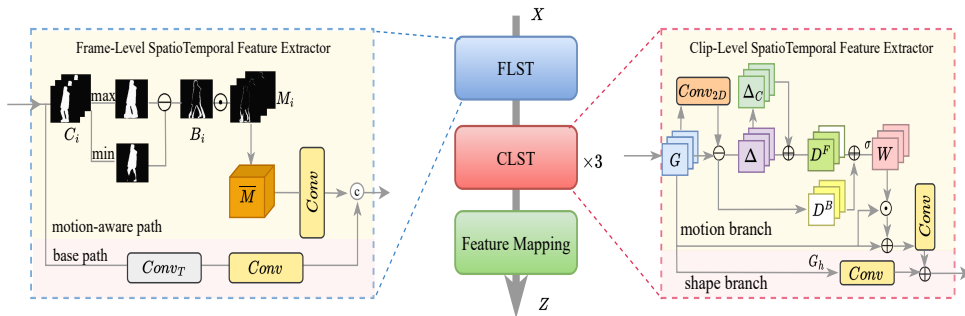


Figure 1: The overall architecture of our proposed GaitMAST network. GaitMAST consists of two main motion-aware modules: frame-level spatiotemporal feature extractor (FLST) and clip-level spatiotemporal feature extractor (CLST).

Figure 1 presents the overall architecture of GaitMAST. The core idea of the proposed GaitMAST is to utilize the motion information on both input and feature level, thus the temporal walking patterns can be well modeled against spatial variations. First, our FLST module takes the silhouette sequences as the input to extract low-level motion-aware feature. Unlike the previous work that has only one path to extract spatiotemporal feature, the shallow layer in our method is a dual-path structure: One extracts the general spatiotemporal feature while the other extracts the *motion-related feature* from the motion sequences. In this manner, the shallow layer can explicitly capture sufficient motion information in the silhouette sequences by fusing the outputs of these two paths. Additionally, frames in one clip are aggregated in the FLST module, indicating the output is the clip-level feature. Second, our deep layers consists of three CLST modules to extract the fine-grained spatiotemporal feature from the clip-level feature.

And each CSTL module has two branches: One focuses on the local spatial details by limiting the increase of receptive field while the other is designed to preserve the motion details by exploring the bi-directional temporal changes. Third, we leverage the widely-used temporal pooling and generalized-mean pooling to aggregate the sequence level feature. Finally, several separate fully connected (FC) layers are employed to map the all part-level gait vectors into metric space for gait recognition.

Before detailing the key modules in GaitMAST, we provide the description of the gait data. We denote a gait sequence of K frames as $\mathbf{X} = [\mathbf{S}_1, \mathbf{S}_2, \dots, \mathbf{S}_K] \in \mathbb{R}^{K \times C \times H \times W}$, where C , H , and W represent the number of color channels, height, and width of one frame \mathbf{S} . Instead of using RGB video frames, the most popular modality used in gait recognition is the silhouette, which is a binary image highlighting the region of the person; correspondingly, $C = 1$ for silhouettes.

2.2 Frame Level Spatiotemporal Feature Extractor

Frame Level Spatiotemporal Feature Extractor (FLST) contains a base path focusing on the whole sequences and a motion-aware path revolving around the dynamic regions in the sequence.

2.2.1 Base path

For the base path, we utilize a commonly-used backbone, which uses one 3D convolution layer of size $3 \times 3 \times 3$ to extract the spatiotemporal feature, followed by another 3D convolution layer of size $3 \times 3 \times 3$ to aggregate the temporal information. More specifically, the base path can be formally defined as:

$$\mathbf{F}^b = \text{Conv}_T(\text{Conv}(\mathbf{X})), \quad (1)$$

where the second 3D convolution Conv_T focuses on aggregating the temporal information through a stride of 3 on the temporal dimension. Here, we use subscript T to indicate that the convolution is focused on temporal information aggregation.

2.2.2 Motion-aware path

For motion-aware path, we first construct the motion sequence and then extract the motion features from it.

Motion sequence construction: Misalignment caused by the limbs' motion is detrimental to spatial feature representation. Nevertheless, the limbs' misalignment embodies the essential walking information conducive to the temporal domain representation. Therefore, we expect to discover the static and dynamic motion information from the binary silhouette regions, according to whether the pixel values in the same position are changed across the temporal dimension. Then the dynamic regions in a silhouette sequence are expected as a motion sequence. Note that 1) in the silhouette generation and pre-processing procedures, there will inevitably produce silhouettes' noises, implying the dynamic regions in the sequence level mistakenly contain those noise pixels. 2) Moreover, body parts alternately move in a walking cycle, indicating that dynamic regions are not continuously changing in the entire sequence. Because of the aforementioned two reasons, it means that selecting the dynamic regions from the local temporal clip will be useful and can alleviate the influence of pseudo-motion information.

More specifically, we uniformly divide a given gait sequence into clips of length L along temporal dimension, which can be formed as $\mathbf{C}_i = [\mathbf{S}_{(i-1)L+1}, \mathbf{S}_{(i-1)L+2}, \dots, \mathbf{S}_{(i-1)L+L}]$, where $i = \{1, 2, \dots, \lfloor K/L \rfloor\}$ is the clip index. Then, the motion region mask \mathbf{B}_i for i -th clip can be generated by

$$\mathbf{B}_i = \max(\mathbf{C}_i) - \min(\mathbf{C}_i), \quad (2)$$

where the \max and \min denotes the maximum and minimum value of one spatial position among L frames for a clip, and $\mathbf{B} \in \mathbb{R}^{H \times W}$. Since the silhouette is binary, when a pixel changes in a clip, the maximum equals 1 and the minimum is 0. For the static pixels, the maximum is equal to the minimum. Thus, the mask value is 0 for the static pixel and 1 for the dynamic pixel. The silhouettes in the same clip share a common mask, while the different clips have different masks.

Obviously, we can get the motion clip by multiplying each silhouette in the clip with their corresponding mask in an element-wise manner, defined as follows:

$$\mathbf{M}_i = \mathbf{B}_i \odot \mathbf{C}_i = [\mathbf{B}_i \mathbf{S}_{(i-1)L+1}, \dots, \mathbf{B}_i \mathbf{S}_{(i-1)L+L}]. \quad (3)$$

Then, concatenating the motion clip along the temporal dimension yields the final motion sequence $\mathbf{M} = [\mathbf{M}_1, \dots, \mathbf{M}_{\lfloor K/L \rfloor}]$.

The constructed motion sequence serves as the supplement input to the original silhouette sequence, which could strengthen the robustness of gait representation against the spatial variants.

Motion feature extraction: In order to extract the clip level motion feature, we first aggregate the frame level motion within a short clip, which is formulated as

$$\overline{\mathbf{M}}_i = A(\mathbf{M}_i), \quad i = 1, 2, \dots, \lfloor K/L \rfloor. \quad (4)$$

Here, the $A(\cdot)$ operation can be instantiated as either statistical functions such as mean and max, or a convolution with the kernel size $L \times 1 \times 1$. Since max operation reverts the motion to the mask and convolution brings in extra parameters, we use $A := \text{mean}$ on local clips. All aggregated motion clip $\overline{\mathbf{M}}_i$ are concatenated on the temporal dimension, *i.e.* $\overline{\mathbf{M}} = [\overline{\mathbf{M}}_1, \dots, \overline{\mathbf{M}}_{\lfloor K/L \rfloor}]$. Subsequently, we feed the aggregated motion sequence $\overline{\mathbf{M}}$ into a 3D convolution layer of size $3 \times 3 \times 3$ to extract the motion feature acquainted with temporal evolution, formulated as:

$$\mathbf{F}^m = \text{Conv}(\overline{\mathbf{M}}). \quad (5)$$

2.2.3 Fusion

The base path pays attention to the salient spatial information, while the motion-aware path revolves around the temporal dynamic information. These mutual complement paths enable the following layer with sufficient spatiotemporal

information. Since the motion region accounts for a part of the silhouette, the motion feature is sparser than the silhouette feature. Accordingly, we concatenate the \mathbf{F}^b and \mathbf{F}^m on channel as the output of the FLST module, avoiding the neglect of temporal changes as the prior work, formulated as

$$\mathbf{G} = \text{Concat}_C(\mathbf{F}^b, \mathbf{F}^m), \quad (6)$$

where Concat with subscript C denotes the matrix concatenation channel dimension.

2.3 Clip Level Spatiotemporal Feature Extractor

The stacked CLST modules in the deep layers aim to extract the high-level semantic feature. Varying from the prior works only concentrating on the spatial scope visible for convolution, we focus on the temporal evolution retention. Thus our CLST module is designed with shape and motion branches to reserve the fine-grained spatial and temporal features.

2.3.1 Shape branch

Currently, the subtle spatial information can be accessed by constraining the receptive field, and part-based convolution has been widely used in cross-view gait recognition. In this fashion, we thus horizontally split the input feature into P parts, $\{\mathbf{G}_h\}_{h=1}^P$. Our shape branch can be formulated as

$$\mathbf{G}^s = \text{Concat}_H(\{\text{Conv}(\mathbf{G}_h)\}_{h=1}^P). \quad (7)$$

2.3.2 Motion branch

On the motion branch, we rescale the input feature based on the exquisite motion information, followed by a convolution layer. The stacked temporal convolution weakens the differences in the temporal dimension, making the motion information hard to model. A natural idea to address this issue is to boost the motion-related information before each temporal convolution operation. Consequently, we recalibrate the feature to capture better motion features. Firstly, we introduce a bi-directional fine and coarse temporal difference module to distill the subtle motion information from the feature volume. The feature-level motion information between two consecutive feature maps can be calculated by temporal difference operation $\Delta(\mathbf{G}_t, \mathbf{G}_{t+1}) = \mathbf{G}_{t+1} - \mathbf{G}_t$,

and the difference is adopted as the motion intensity. However, this operation may vanish some motion information where the position value is constant but the semantic context changes. In order to enlarge the movement search space, we intend to conduct spatial convolution on features. Furthermore, considering different channels focus on different levels of spatial and temporal information [16], channel-wise convolution is employed here. The temporal difference is formulated as:

$$\Delta(\mathbf{G}_t, \mathbf{G}_{t+1}) = \text{Conv}_{2D}(\mathbf{G}_{t+1}) - \mathbf{G}_t, \quad (8)$$

where Conv_{2D} denotes 2D convolution of size 3×3 . Take a single channel for example, the convolution kernel element $w_{i,j}$ semantically represents the importance of different motional movement directions (i, j) . The larger the value, the higher the degree of attention to the motion in direction. Since the element-wise deviation provides the fine-grained motion information, we summarize the spatial information as a coarse motion by global average pooling:

$$\Delta_C(\mathbf{G}_t, \mathbf{G}_{t+1}) = \text{GAP}_{WH}(\Delta(\mathbf{G}_t, \mathbf{G}_{t+1})), \quad (9)$$

where GAP with subscript WH denotes global average pooling along width and height dimensions. Moreover, we utilize bi-directional temporal difference, forward $\Delta(\mathbf{G}_t, \mathbf{G}_{t+1})$ and backward $\Delta(\mathbf{G}_{t+1}, \mathbf{G}_t)$, to enhance the richness of motion information expression. Overall, the temporal difference results are formulated as follows:

$$\begin{cases} \mathbf{D}_t^F = \Delta(\mathbf{G}_t, \mathbf{G}_{t+1}) + \Delta_C(\mathbf{G}_t, \mathbf{G}_{t+1}), \\ \mathbf{D}_t^B = \Delta(\mathbf{G}_{t+1}, \mathbf{G}_t) + \Delta_C(\mathbf{G}_{t+1}, \mathbf{G}_t). \end{cases} \quad (10)$$

Here the superscripts F and B denote the forward and backward operations respectively. We note that the last frame and first frame are not involved in the forward direction and backward direction, respectively. For the convenience of computation, we pad a zero matrix $\mathbf{0}$ on the corresponding position, and concatenate the temporal differences along the temporal dimension yielding the temporal difference sequence: $\mathbf{D}^F = [\mathbf{D}_1^F, \dots, \mathbf{D}_{[K/L]-1}^F, \mathbf{0}]$, and $\mathbf{D}^B = [\mathbf{0}, \mathbf{D}_2^B, \dots, \mathbf{D}_{[K/L]}^B]$.

Secondly, we recalibrate the module guided by motion information. A sigmoid function σ is utilized to map the motion intensity into range $(0, 1)$, yielding the average attention from forward and backward directions:

$$\mathbf{W} = (\sigma(\mathbf{D}^F) + \sigma(\mathbf{D}^B))/2 - 1/2. \quad (11)$$

Here, we minus 0.5 to set the motion intensity as 0 since there is no backward motion in the first frame and no forward motion in the last frame. When conducting recalibration, the input feature performs addition with the motion feature, which is the element-wise product of the input feature and motion-aware attention, followed by a convolutional layer to extract motion-aware spatiotemporal feature:

$$\mathbf{G}^m = \text{Conv}(\mathbf{G} + \mathbf{G} \odot \mathbf{W}). \quad (12)$$

2.3.3 Fusion

Consequently, fusing the outcome of shape and motion branches brings about the output of the CLST module:

$$\mathbf{G}_{next} = \text{fusion}(\mathbf{G}^s, \mathbf{G}^m). \quad (13)$$

Here, we select summation and concatenation as two fusion candidates. There are three CSTL modules in our network. The output of the first two modules is marked as \mathbf{G}_{next} , and the output of the last CSLT denotes \mathbf{G}_{last} that are sent to the feature mapping stage.

2.4 Feature Mapping and Loss Function

To obtain the sequence level feature representation, we employ temporal pooling to aggregate the clip feature, implemented by global temporal maxpooling, followed by generalized-mean pooling (GeM) for spatial pooling [17]. Afterward, we utilize separate fully connection layer and batch normalization layer to map the feature \mathbf{Z} into a metric space:

$$\mathbf{Z} = \text{BN}\left(\text{FC}\left(\left[\text{GAP}_W\left(\left[\text{GAP}_T(\mathbf{G}_{last})\right]^q\right)\right]^{\frac{1}{q}}\right)\right). \quad (14)$$

where GAP_W and GAP_T denote the global average pooling along width dimension and temporal dimension, respectively. Here q is a hyperparameter to be manually set. It degrades to max pooling when $q \rightarrow \infty$ and average pooling for $q = 1$.

Following GaitGL [9], we use triplet loss and cross entropy loss function to optimize GaitMAST.

2.5 Training and Testing

The ordered silhouette sequences are fed to the proposed network in the training and testing phases. During the training phase, the length of sequences is set to 30. We randomly select p identities with k sequences to construct a mini-batch containing $p \times k$ sequences. During the test phases, the length of sequences is not fixed but all the frames are sent to the network. The evaluation criterion is rank-1 accuracy, and the Euclidean distance is used to measure the distances between one probe and candidates in the gallery.

3 Experiments

In this section, we will introduce two gait datasets, implementation details, experimental results and conduct several ablation experiments on the CASIA-B dataset to testify every innovation’s effectiveness.

3.1 Datasets

CASIA-B dataset [18] is a widely used dataset containing 124 individuals. There are 11 camera-perspective uniformly sampling from range $(0^\circ, 180^\circ)$ with 10 sequences in 3 walking conditions for each individual. Normal status (NM) has 6 sequences, bag carrying (BG) and coat-wearing (CL) have 2 sequences respectively. Under the subject-independent protocol, there are 3 division plans including small-sample training (ST), middle-sample training (MT) and large-sample training (LT) with different training sets size. The ST setting takes 0 – 24 individuals as the training set, and the rest data set as test set. The training data set size in MT and LT is 62 and 74 respectively. During the testing phase, we regard the first four sequences in NM condition as gallery.

OU-MVLP is one of the biggest cross-view dataset [20] with 10, 307 individuals. There are 14 views sampling from $(0^\circ, 90^\circ)$ and $(270^\circ, 360^\circ)$ respectively per subject and 2 sequences ($\#seq - 00, \#seq - 01$) per view. The train data contains 5, 153 individuals, another 5, 154 individuals are taken as test data. In the testing phase, we set $\#seq - 01$ as gallery data.

Gallery NM#1-4		0°-180°													
Probe		0°	18°	36°	54°	72°	90°	108°	126°	144°	162°	180°	mean		
ST (24)	NM#5-6	MT3D	71.9	83.9	90.9	90.1	81.1	75.6	82.1	89.0	91.1	86.3	69.2	82.8	
		GaitGL	77.0	87.8	93.9	92.7	83.9	78.7	84.7	91.5	92.5	89.3	74.4	86.0	
		GaitMAST	81.6	91.1	96.4	93.8	84.1	80.0	85.5	92.9	94.7	91.1	78.6	88.1	
	BG#1-2	MT3D	64.5	76.7	82.8	82.8	73.2	66.9	74.0	81.9	84.8	80.2	63.0	74.0	
		GaitGL	68.1	81.2	87.7	84.9	76.3	70.5	76.1	84.5	87.0	83.6	65.0	78.6	
		GaitMAST	73.8	85.5	91.3	87.7	76.1	71.2	78.8	86.9	89.9	86.3	71.3	81.7	
	CL#1-2	MT3D	46.6	61.6	66.5	63.3	57.4	52.1	58.1	58.9	58.5	57.4	41.9	56.6	
		GaitGL	46.9	58.7	66.6	65.4	58.3	54.1	59.5	62.7	61.3	57.1	40.6	57.4	
		GaitMAST	54.9	69.3	76.4	73.0	65.2	58.1	65.7	71.6	71.8	66.0	47.1	65.4	
MT (62)	NM#5-6	MT3D	91.9	96.4	98.5	95.7	93.8	90.8	93.9	97.3	97.9	95.0	86.8	94.4	
		GaitGL	93.9	97.6	98.8	97.3	95.2	92.7	95.6	98.1	98.5	96.5	91.2	95.9	
		GaitMAST	94.4	98.2	99.0	98.2	96.1	93.6	97.2	98.6	99.0	97.7	93.6	96.9	
	BG#1-2	MT3D	86.7	92.9	94.9	92.8	88.5	82.5	87.5	92.5	95.3	92.9	81.2	89.8	
		GaitGL	88.5	95.1	95.9	94.2	91.5	85.4	89.0	95.4	97.4	94.3	86.3	92.1	
		GaitMAST	90.3	96.1	97.5	96.3	93.3	90.3	92.9	96.5	98.4	96.0	89.4	94.3	
	CL#1-2	MT3D	67.5	81.0	85.0	80.6	75.9	69.8	76.8	81.0	80.8	73.8	59.0	75.6	
		GaitGL	70.7	83.2	87.1	84.7	78.2	71.3	78.0	83.7	83.6	77.1	63.1	78.3	
		GaitMAST	72.4	89.7	92.8	89.6	83.2	79.0	83.9	89.2	90.7	84.8	66.5	83.8	
LT (74)	NM#5-6	GaitSet	90.8	97.9	99.4	96.9	93.6	91.7	95.0	97.8	98.9	96.8	85.8	95.0	
		GaitPart	94.1	98.6	99.3	98.5	94.0	92.3	95.9	98.4	99.2	97.8	90.4	96.2	
		MT3D	95.7	98.2	99.0	97.5	95.1	93.9	96.1	98.6	<u>99.2</u>	98.2	92.0	96.7	
		GaitG	96.0	98.3	99.0	97.9	96.9	95.4	97.0	98.9	99.3	98.8	94.0	97.4	
		CSTL	97.2	99.0	99.2	98.1	96.2	95.5	<u>97.7</u>	98.7	99.2	98.9	96.5	97.8	
		Gaitstrip [†]	96.0	98.4	98.8	97.9	96.6	95.3	97.5	98.9	99.1	99.0	96.3	97.6	
		GaitMAST	96.3	98.8	99.1	98.1	97.2	96.5	98.2	99.1	99.3	99.2	95.9	98.0	
		BG#1-2	GaitSet	83.8	91.2	91.8	88.8	83.3	81.0	84.1	90.0	92.2	94.4	79.0	87.2
			GaitPart	89.1	94.8	96.7	95.1	88.3	84.9	89.0	93.5	96.1	93.8	85.8	91.5
	MT3D		91.0	95.4	97.5	94.2	92.3	86.9	91.2	95.6	97.3	96.4	86.6	93.0	
	GaitGL		92.6	96.6	96.8	95.5	93.5	89.3	92.2	96.5	98.2	96.9	91.5	94.5	
	CSTL		91.7	<u>96.5</u>	97.0	95.4	90.9	88.0	91.5	95.8	97.0	95.5	90.3	93.6	
	Gaitstrip [†]		92.8	96.6	97.2	96.5	95.2	90.5	93.5	97.5	98.3	97.6	91.4	95.2	
	GaitMAST		93.7	96.4	<u>97.4</u>	97.2	96.2	93.4	95.5	97.8	98.4	97.8	93.1	96.1	
	CL#1-2		GaitSet	61.4	75.4	80.7	77.3	72.1	70.1	71.5	73.5	73.5	68.4	50.0	70.4
			GaitPart	70.7	85.5	86.9	83.3	77.1	72.5	76.9	82.2	83.8	80.2	66.5	78.7
		MT3D	76.0	87.6	89.8	85.0	81.2	75.7	81.0	84.5	85.4	82.2	68.1	81.5	
		GaitGL	76.6	90.0	90.3	87.1	84.5	79.0	84.1	87.0	87.3	84.4	69.5	83.6	
CSTL		78.1	89.4	91.6	86.6	82.1	79.7	81.8	86.3	88.7	86.6	75.3	84.2		
Gaitstrip [†]		79.9	92.3	93.4	89.2	86.0	80.0	86.0	88.5	91.7	87.5	73.5	86.2		
GaitMAST		79.6	93.4	95.0	92.4	88.4	82.5	86.9	91.4	93.9	90.1	75.3	88.1		

Table 1: Averaged rank-1 accuracies on CASIA-B under three different experimental settings, excluding identical-view cases. Superscript [†] marks the work [19] available on arXiv.

Method	Probe view													Mean	
	0°	15°	30°	45°	60°	75°	90°	180°	195°	210°	225°	240°	255°		270°
GaitSet*	78.7	87.4	89.8	90.0	87.8	88.5	97.5	81.3	86.2	88.9	89.1	87.1	87.6	86.1	86.9
GaitPart*	82.1	88.8	90.7	90.8	89.5	89.7	89.1	84.7	87.4	89.9	90.0	88.7	88.9	87.8	88.4
GaitGL*	84.3	89.9	<u>91.1</u>	91.4	<u>90.9</u>	90.6	90.2	<u>88.3</u>	<u>88.1</u>	<u>90.3</u>	<u>90.4</u>	<u>89.6</u>	89.4	88.6	<u>89.5</u>
GaitMAST	87.1	91.0	91.4	91.8	91.7	91.3	91.1	90.3	89.6	90.7	90.8	90.5	90.2	89.9	90.5

Table 2: Averaged rank-1 on OUMVLP under 14 probe views excluding identical-view cases. The superscript * notes the average rank-1 accuracies are reproduced results in our test sets for a fair comparison.

3.2 Implementation Details

The gait silhouettes is normalized before being fed to the network, and the input size is set to 64×44 . And the batch size (p, k) is $(8, 8)$ in CASIA-B dataset and $(16, 8)$ in OU-MVLP dataset, respectively. In our GaitMAST network, we have one FLST block and three CLST blocks. The number of output channel are 32, 128, 256, 256 for each block respectively. Since the OU-MVLP is 20 times bigger than CASIA-B, we directly increases the convolution layers up to 2 of three CLST modules instead of stacking more modules when training on OU-MVLP. Considering the increment of convolution layers, we add a spatial pooling layer after the second CLST module. Additionally, as the big dataset requires more fine-grained features to distinguish the different subjects, we add a $1 \times 1 \times 1$ convolution layer for channel information interaction after the FLST. The output channels of each convolution layer are 32, 32, 64, 128, 128, 256, 256, 512, 512. In the training stage, the batch size is $(32, 8)$, which is equal to the prior works [9, 12]. As for the spatial fine-grained pathway in CLST block, the part number is set to 8 following the configuration in prior work [9]. The final fusion of

Methods	NM	BG	CL	Mean
GaitGL	97.4	94.5	83.6	91.8
CSTL	97.8	93.6	84.2	91.9
GaitMAST	98.0	96.1	88.1	94.1
w/o FLST	97.2	94.7	84.3	92.1
w/o CLST	98.1	95.8	87.0	93.6

Table 3: The ablation study of motion information used in different spatiotemporal feature extractor modules (FLST and CLST).

the CLST is summation in the first two modules, and the third is implemented by concatenating them horizontally. The hyperparameter q in GeM is 6.5. The optimizer is set as Adam [21] and learning rate is 0.0001 in all experiment. For experiments on CASIA-B, the weight decay set to 0.0005. The training iterations set to 70k, 80k, 80k for ST, MT and LT configuration. For the LT training, the learning rate decay to 0.00001 after 70k. For the OU-MVLP, the total iterations are 90k, and the learning rate decay to $1e - 5$ after 80k. The margin of triplet loss in all experiment set to 0.2. We use four NVIDIA GeForce RTX 3090 GPUs for training GaitMAST.

3.3 Comparison with the State-of-the-art Method

In this section, we compare the proposed GaitMAST with other state-of-the-art methods on CASIA-B and OU-MVLP datasets, and the results are shown on Table 1 and Table 2.

Following the dataset scales protocol in [7] of CASIA-B, we test our GaitMAST in ST, MT and LT settings in all views and clothing conditions. From Table 1 it can be seen that the average rank-1 accuracies in ST, MT and LT are 78.4%, 91.7% and 94.1%, with 4.4%, 2.9% and 2.3% corresponding improvements for every condition compared with one of the leading methods GaitGL [9]. Concretely, GaitMAST achieves 98.0%, 96.1%, 88.1% average rank-1 accuracies in the NM, BG, and CL conditions under the LT settings, which outperforms GaitGL by 0.6%, 1.6% and 4.5% and implies the superiority of GaitMAST. It is worth noting that even our GaitMAST trained under MT exceeds MT3D [13] 1.3 % trained with LT in terms of average rank-1 accuracy, showing the high capacity of GaitMAST. When testing on OU-MVLP, the experimental results reach 90.6% averaged rank-1 accuracy on all views. When discarding the illegal sequences, the average rank-1 accuracy will rise to 97.1%. The evaluation results prove the generalization capacity of our method. From the above table, we can find the rank-1 accuracies of 0° , 15° , 180° , 195° , 240° , 255° , and 270° of GaitGL are lower than 90%, indicating these viewpoints are more difficult than others. Nevertheless, our GaitMAST achieves a large margin improvement on these viewpoint. A possible reason is that the motion information offers improvements, further suggesting that the motion-aware network benefits gait recognition.

Cross-view evaluation: There are apparent performance gaps between different views, indicating that the feature representation is vulnerable to the view. Nevertheless, our GaitMAST reduces the gap between various views (refer to Table s1 in supplementary materials), especially from 8.9% to 5.3% in the case of BG, demonstrating the robustness to view changes. Further, the worst view lies among 0° , 90° , or 180° . A possible reason is that these views sacrifice part of the gait information. However, we argue that awaring motion can bridge the gap since specific body parts' motions are salient. Noteworthy, the performance on 90° has been upgraded by our GaitMAST, exceeding the start-of-the-art results by 1.0% (NM), 2.9% (BG) and 2.5% (CL) since the evident legging movement benefits GaitMAST. Furthermore, we curve the rank-1 accuracies for all views on NM, BG, and CL under the LT setting of CASIA-B, shown on Figure 2

Evaluation in different clothing conditions: The clothing condition is another factor that affects the test performance. Generally, BG and CL are harder than NM. Nevertheless, our GaitMAST achieves apparent gains in both problematic conditions, referring to Table s2 in supplementary materials. The performance degradation from NM to CL is 9.9%, which is smaller than the state-of-the-art methods and means our GaitMAST is robust to the clothing changes. Moreover, the performance in different views except 0° and 180° is considerably improved 4.4% than GaitGL in the case of CL, indicating the GaitMAST has a strong representation ability under challenging conditions.

3.4 Ablation Studies

Effect of the GaitMAST network: The core idea of the GaitMAST is that motion could facilitate the feature representation ability. Therefore, two motion-aware modules, including FLST and CLST, are proposed to capture the motion-related information. To explore the contributions of these two modules, we design the ablation studies under LT settings and draw an apple-to-apple comparison with other spatiotemporal representation models, presented in Table 3. It is worth noting that the proposed GaitMAST outperforms others, even only leaving one motion-aware module. The CLST-styled GaitMAST improves 0.2% over other methods, and the FLST-styled GaitMAST advances

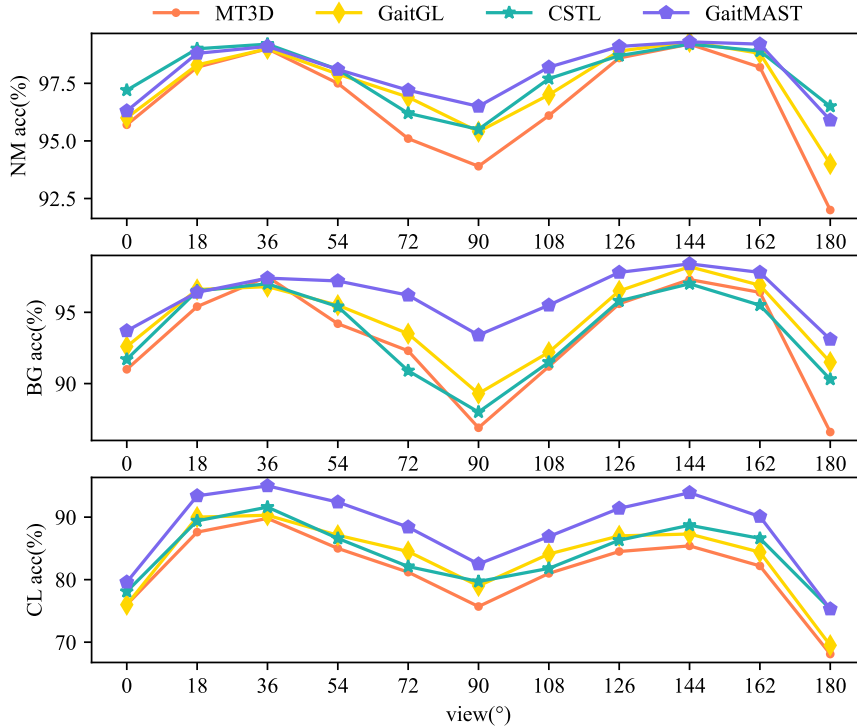


Figure 2: The performance comparison of different clothing conditions under the LT setting.

1.7%. More importantly, the accuracy remarkably increases 2.2% using both two modules. Note that GaitGL and CSTL model on temporal dimension with shared parameter over the feature volume. Although 3DLocal tries to employ body parts-specific 3D convolution blocks, it does not break the convolution’s property of parameters sharing on the temporal dimension; hence diversity of motion cannot be well represented. Nevertheless, our CLST module conducts element-adaptive motion attention based on the motion intensity, bringing out the richness of temporal modeling. Comparing the designed FLST and CLST, we observe that the FLST is more effective than the CLST, increasing 1.5% accuracy. The possible reason is that the motion information is missed by the smoothed effect of convolution as the network deepens. Therefore, although it boosts the motion-related element, it is hard to capture efficient motion information as the input silhouette sequences.

Analysis of the FLST: Following the mask generation manner, we conduct experiments to study the different implementation methods in generating motion sequences. First, we analyze the effect of the clip length on results, shown in Table 4. The average rank-1 accuracy degrades from 94.1% to 92.5% when the clip length increases from 3 to 5. When the length grows to 6, the results show that the performance drop from 92.5% to 91.7%. This phenomenon may be due to increased local temporal pseudo-motion information in the motion sequence when the clip length grows. Second, we also conduct ablation studies on aggregation methods. In Table 4 the results shows the the statistical function $\text{mean}(\cdot)$ is better than $\text{max}(\cdot)$ and convolution, indicating that our aggregation strategy is effective.

Analysis of the CLST: The core idea in CLST is to recalibrate the feature by the motion information. Therefore, we conduct several experiments investigating temporal difference objections, motion granularities, and the effectiveness of bi-directional motion information. As shown in the Table 5, directly operating temporal difference on feature volume drops the performance from 94.1% to 93.3%, implying that enlarging the motion search space in deep layers is beneficial. It is observed that only conducting frame-level feature re-calibration may hurt the performance. The coarse motion tends to be indiscriminative since individuals share the same action, walking. However, when employing both fine and coarse motion, the performance can be improved 1.0%. The fine-coarse motion rescaling mechanism is similar to the walking characters in that the motion is diverse in different body parts and timesteps. Further, the bi-directional motion is better than single forward motion by 0.3%, indicating that adequate motion information is conducive to the expression of gait representation.

		Rank-1 Accuracy			
		NM	BG	CL	Mean
Length	3	98.0	96.1	88.1	94.1
	5	97.5	94.8	85.3	92.5
	6	97.2	94.6	83.3	91.7
Aggregation	mean	98.0	96.1	88.1	94.1
	conv	97.9	95.8	88.1	94.0
	max	97.7	95.7	87.8	93.8

Table 4: The different choices on the clip length and feature aggregation methods in the FLST module.

Conv	MG		BD	Rank-1 Accuracy			
	F	C		NM	BG	CL	Mean
	✓	✓	✓	97.9	95.5	86.5	93.3
✓	✓		✓	98.0	95.7	87.1	93.6
✓		✓	✓	97.9	95.6	85.7	93.1
✓	✓	✓		97.9	95.8	87.6	93.8
✓	✓	✓	✓	98.0	96.1	88.1	94.1

Table 5: The overall ablation studies of the temporal difference operation, the motion granularity (MG, fine-grained (F) and coarse-grained (C)), and the bi-directional (BD) motion information utilization.

4 Conclusion

This paper proposed a novel motion-aware spatiotemporal feature learning network for cross-view gait recognition. Unlike the prior work, we take advantage of diverse motion patterns in the silhouette sequences. Concretely, we design two motion-aware modules: the frame-level spatiotemporal feature extractor (FLST) in the shallow layer paying attention to the whole and dynamic regions, and clip-level spatiotemporal feature extractor (CLST) in the deeper layers focusing on fine-grained information in both spatial and temporal domains. Extensive experimental results demonstrate the superiority of our motion-aware method. In the future, how to use high-frame rate camcorder to collect a high-frame gait dataset for better utilizing the potential of motion features deserves studying.

References

- [1] Rijun Liao, Chunshui Cao, Edel B Garcia, Shiqi Yu, and Yongzhen Huang. Pose-based temporal-spatial network (ptsn) for gait recognition with carrying and clothing variations. In *Chinese Conference on Biometric Recognition*, pages 474–483, 2017.
- [2] Xiang Li, Yasushi Makihara, Chi Xu, Yasushi Yagi, Shiqi Yu, and Mingwu Ren. End-to-end model-based gait recognition. In *Proceedings of the Asian Conference on Computer Vision*, 2020.
- [3] Rijun Liao, Shiqi Yu, Weizhi An, and Yongzhen Huang. A model-based gait recognition method with body pose and human prior knowledge. *Pattern Recognition*, 98:107069, 2020.
- [4] Ju Han and Bir Bhanu. Individual recognition using gait energy image. *IEEE Trans. Pattern Anal. Mach. Intell.*, 28(2):316–322, 2006.
- [5] Khalid Bashir, Tao Xiang, and Shaogang Gong. Gait recognition using gait entropy image. In *3rd International Conference on Imaging for Crime Detection and Prevention*, pages 1–6, 2009.
- [6] Chen Wang, Junping Zhang, Jian Pu, Xiaoru Yuan, and Liang Wang. Chrono-gait image: A novel temporal template for gait recognition. In *11th European Conference on Computer Vision*, pages 257–270, 2010.
- [7] Hanqing Chao, Yiwei He, Junping Zhang, and Jianfeng Feng. Gaitset: Regarding gait as a set for cross-view gait recognition. In *The Thirty-Third AAAI Conference on Artificial Intelligence*, pages 8126–8133, 2019.
- [8] Chao Fan, Yunjie Peng, Chunshui Cao, Xu Liu, Saihui Hou, Jiannan Chi, Yongzhen Huang, Qing Li, and Zhiqiang He. Gaitpart: Temporal part-based model for gait recognition. In *Proceedings of the IEEE/CVF Conference on Computer Vision and Pattern Recognition*, pages 14213–14221, 2020.
- [9] Beibei Lin, Shunli Zhang, and Xin Yu. Gait recognition via effective global-local feature representation and local temporal aggregation. In *Proceedings of the IEEE/CVF International Conference on Computer Vision*, pages 14628–14636, 2021.

- [10] Ziyuan Zhang, Luan Tran, Xi Yin, Yousef Atoum, Xiaoming Liu, Jian Wan, and Nanxin Wang. Gait recognition via disentangled representation learning. In *Proceedings of the IEEE/CVF Conference on Computer Vision and Pattern Recognition*, pages 4710–4719, 2019.
- [11] Yuqi Zhang, Yongzhen Huang, Shiqi Yu, and Liang Wang. Cross-view gait recognition by discriminative feature learning. *IEEE Trans. Image Process.*, 29:1001–1015, 2020.
- [12] Xiaohu Huang, Duowang Zhu, Hao Wang, Xinggong Wang, Bo Yang, Botao He, Wenyu Liu, and Bin Feng. Context-sensitive temporal feature learning for gait recognition. In *Proceedings of the IEEE/CVF International Conference on Computer Vision*, pages 12889–12898, 2021.
- [13] Beibei Lin, Shunli Zhang, and Feng Bao. Gait recognition with multiple-temporal-scale 3d convolutional neural network. In *The 28th ACM International Conference on Multimedia*, pages 3054–3062, 2020.
- [14] Zhen Huang, Dixiu Xue, Xu Shen, Xinmei Tian, Houqiang Li, Jianqiang Huang, and Xian-Sheng Hua. 3D local convolutional neural networks for gait recognition. In *Proceedings of the IEEE/CVF International Conference on Computer Vision*, pages 14920–14929, 2021.
- [15] Yunpeng Zhang, Zhengyou Wang, Shanna Zhuang, and Hui Wang. Motion gait: Gait recognition via motion excitation. *arXiv preprint arXiv:2206.11080*, 2022.
- [16] Boyuan Jiang, MengMeng Wang, Weihao Gan, Wei Wu, and Junjie Yan. Stm: Spatiotemporal and motion encoding for action recognition. In *Proceedings of the IEEE/CVF International Conference on Computer Vision*, pages 2000–2009, 2019.
- [17] Filip Radenović, Giorgos Tolias, and Ondřej Chum. Fine-tuning cnn image retrieval with no human annotation. *IEEE Trans. Pattern Anal. Mach. Intell.*, 41(7):1655–1668, 2018.
- [18] Shiqi Yu, Daoliang Tan, and Tieniu Tan. A framework for evaluating the effect of view angle, clothing and carrying condition on gait recognition. In *18th International Conference on Pattern Recognition*, volume 4, pages 441–444, 2006.
- [19] Ming Wang, Beibei Lin, Xianda Guo, Lincheng Li, Zheng Zhu, Jiande Sun, Shunli Zhang, and Xin Yu. Gaitstrip: Gait recognition via effective strip-based feature representations and multi-level framework. *arXiv preprint arXiv:2203.03966*, 2022.
- [20] Noriko Takemura, Yasushi Makihara, Daigo Muramatsu, Tomio Echigo, and Yasushi Yagi. Multi-view large population gait dataset and its performance evaluation for cross-view gait recognition. *IPSJ Transactions on Computer Vision and Applications*, 10(1):1–14, 2018.
- [21] Diederik P Kingma and Jimmy Ba. Adam: A method for stochastic optimization. *arXiv preprint arXiv:1412.6980*, 2014.